NeuroImage: Clinical 3 (2013) 290–300

Contents lists available at ScienceDirect

NeuroImage: Clinical

journal homepage: www.elsevier.com/locate/ynicl

Impaired structural correlates of memory in Alzheimer's disease mice ☆

AmanPreet Badhwar [a,1], Jason P. Lerch [b,c,1], Edith Hamel [a,*], John G. Sled [b,c,**]

[a] Laboratory of Cerebrovascular Research, Montreal Neurological Institute, McGill University, Montréal, QC H3A 2B4, Canada
[b] Mouse Imaging Centre, Hospital for Sick Children, Toronto, ON M5T 3H7, Canada
[c] Department of Medical Biophysics, University of Toronto, Toronto, ON M5G 2M9, Canada

ARTICLE INFO

Article history:
Received 20 June 2013
Received in revised form 14 August 2013
Accepted 30 August 2013
Available online xxxx

Keywords:
Alzheimer's disease
Mouse model
Magnetic resonance imaging
Memory
Neuroanatomical plasticity
Pioglitazone-treatment

ABSTRACT

The healthy adult brain demonstrates robust learning-induced neuroanatomical plasticity. While altered neuroanatomical plasticity is suspected to be a factor mitigating the progressive cognitive decline in Alzheimer's disease (AD), it is not known to what extent this plasticity is affected by AD. We evaluated whether spatial learning and memory-induced neuroanatomical plasticity are diminished in an adult mouse model of AD (APP mice) featuring amyloid beta-driven cognitive and cerebrovascular dysfunction. We also evaluated the effect of early, long-term pioglitazone-treatment on functional hyperemia, spatial learning and memory, and associated neuroanatomical plasticity. Using high-resolution post-mortem MRI and deformation-based morphometry, we demonstrate spatial learning and memory-induced focal volume increase in the hippocampus of wild-type mice, an effect that was severely attenuated in APP mice, consistent with their unsuccessful performance in the spatial Morris water maze. These findings implicate impaired neuroanatomical plasticity as an important contributing factor to cognitive deficits in the APP mouse model of AD. Pioglitazone-treatment in APP mice completely rescued functional hyperemia and exerted beneficial effects on spatial learning and memory-recall, but it did not improve hippocampal plasticity.

1. Introduction

Spatial learning and recall are disrupted early in the course of Alzheimer's disease (AD) and worsen with disease progression (Amieva et al., 2005; Henderson et al., 1989). A potential mechanism that may contribute to these deficits is loss of learning and memory-induced neuroanatomical plasticity. The anatomical structure of the healthy adult human brain is plastic, and demonstrates both short- and long-term learning-induced remodeling that is detectable as volumetric differences on MRI (Draganski et al., 2004; Maguire et al., 2000). Specifically, neuroanatomical plasticity in response to long-term spatial learning and recall was demonstrated in successful London taxi driver trainees, who at the end of their training demonstrated greater grey matter (GM) volume in the posterior hippocampi compared to unsuccessful trainees and non-taxi-driving controls (Woollett and Maguire, 2011). Recently, using high-resolution in situ post-mortem MRI and deformation-based morphometry (DBM), we showed specific growth in the dorsal hippocampus (equivalent to posterior hippocampus in human) of mice trained for five days on the spatial Morris water maze (MWM) (Lerch et al., 2011a). To date, it is not known to what extent learning and memory-induced hippocampal plasticity is affected in transgenic mouse models of AD.

Cerebral blood flow (CBF) insufficiency has been associated with altered learning and memory (Iadecola, 2004). Its early appearance in AD has raised the question as to whether hypoperfusion contributes to the cognitive decline (Zlokovic et al., 2005). Cognitive task-induced regional CBF increase is attenuated in at-risk individuals (Xu et al., 2007) and in AD patients (Peters et al., 2009). These observations, and the finding that CBF insufficiency can negate the effects of memory enhancing agents (Yoshida et al., 2007), suggest that therapy that improves CBF and leads to a better blood supply to neurons could potentially improve memory in AD (Li et al., 2011; Yoshida et al., 2007).

One such candidate is the drug pioglitazone, an agonist at the peroxisome proliferator-activated receptor gamma (PPARγ). Pioglitazone is safe to administer to AD patients (Geldmacher et al., 2011) and was shown to improve cognition and cerebral perfusion in mild AD patients with type II diabetes mellitus (T2DM) (Sato et al., 2009). We demonstrated in elderly AD mice that short-term pioglitazone-treatment normalized cerebrovascular function, but not cognitive performance, possibly due to short treatment duration and the very late stage of the pathology (Nicolakakis et al., 2008). Given that pioglitazone was also able to blunt cerebral oxidative stress, glial activation, and cholinergic denervation, processes strongly associated with AD, we suggested that

* Correspondence to: E. Hamel, Laboratory of Cerebrovascular Research, Montreal Neurological Institute, Montréal, QC H3A 2B4, Canada. Tel.: +1 514 398 8928; fax: +1 514 398 8106.
** Correspondence to: J.G. Sled, Mouse Imaging Centre, Toronto Centre for Phenogenomics, Toronto, ON M5T 3H7, Canada. Tel.: +1 647 837 5818; fax: +1 647 837 5832.
E-mail addresses: edith.hamel@mcgill.ca (E. Hamel), john.sled@utoronto.ca (J.G. Sled).
[1] Contributed equally.

2213-1582/$ – see front matter © 2013 The Authors. Published by Elsevier Inc. All rights reserved.
http://dx.doi.org/10.1016/j.nicl.2013.08.017

a favorable response on memory might be elicited by earlier and longer treatment. In the current study, we assess whether spatial learning and memory-related neuroanatomical plasticity is diminished in adult APP mice, and whether early-initiated, long-term pioglitazone-treatment improves cerebrovascular function, cognitive performance and neuroanatomical plasticity.

2. Materials and methods

2.1. Mice

Transgenic mice overexpressing a mutated form of the human amyloid precursor protein (APP mice, line J20) and their wildtype (WT) littermates (C57BL/6J) were used in this study. The APP/J20 line carries one copy of the familial early-onset AD Swedish ($670/671_{KM \rightarrow NL}$) and Indiana ($717_{V \rightarrow F}$) APP mutations on the C57BL/6J background (Mucke et al., 2000). The transgene is driven by the platelet-derived growth factor β promoter, which leads to increased production of APP-derived amyloid beta (Aβ) peptides. To eliminate sex-associated differences in brain structure, and potential estrus-cycle-related effects on working memory, only males were used. A total of 135 mice were employed, in particular, 58 APP mice and 77 WT littermates. Mice were housed under a 12-hour light-dark cycle, in a temperature (23 °C) and humidity (50%) controlled room, with food and tap water available ad libitum. All experiments were performed in compliance with the Animal Ethics Committee of the Montreal Neurological Institute (MNI) and the guidelines of the Canadian Council on Animal Care.

2.2. Drug treatment

A 14 week treatment regime was initiated in ~3-month-old mice (young mice), an age when Aβ deposition in brain parenchyma is absent (Mucke et al., 2000). The treated group, consisting of approximately half the mice (n = 59; WT(pio), APP(pio)), received a pioglitazone-containing-diet (20 mg/kg/day), while the remaining mice (n = 63; WT, APP) received non-medicated control diet. In addition, to determine the early effect of pioglitazone on cerebrovascular function, a 3-day treatment regime was carried out in a small cohort of young mice (n = 13).

2.3. Laser Doppler flowmetry

Laser Doppler flowmetry (LDF) measurements (Transonic Systems Inc., Ithaca, NY) of evoked CBF change (CBF) in the somatosensory area of the neocortex in response to sensory stimulation were carried out as previously described (Nicolakakis et al., 2008) in two separate cohorts of young (3-month-old) and adult (6-month-old) mice. Activity-induced increase in CBF was measured in young mice (8 WT, 5 APP) before and after 3-day pioglitazone-treatment to determine (a) if APP overexpression induced cerebrovascular insufficiency is present in young APP mice, and (b) whether pioglitazone counters this impairment early during the course of treatment. Activity-induced increase in CBF was measured in adult mice (5 WT, 5 WT(pio), 5 APP, and 4 APP(pio)), where the treated groups received 3-months of pioglitazone, to determine (a) if cerebrovascular insufficiency is persistent, and (b) whether long-term pioglitazone-treatment rescues this insufficiency. We use the level of activity-induced increase in CBF as a marker of global cerebrovascular performance. Anesthetized mice (ketamine 85 mg/kg, intra-muscular (i.m.) and xylazine 3 mg/kg, i.m, Wyeth, St-Laurent QC, Canada) were fixed in a stereotaxic frame and the bone over the barrel cortex was thinned to translucency for positioning of the laser probe. Body temperature was maintained at 37 °C using a heating pad. Changes in CBF before, during, and after unilateral whisker stimulation (3–6 stimulations, 20 s at 8–10 Hz) were recorded, with four to six recordings acquired every 30–40 s and averaged for each mouse. Contralateral CBF change was expressed as percentage increase relative to baseline.

2.4. Morris water maze (MWM) training

At the end of treatment, two separate cohorts of mice were tested for 5 consecutive days in a circular pool (140 cm diameter) filled with water (17 °C ± 1 °C) made opaque with white non-toxic pigment. A third cohort of mice (15 WT, 13 WT(pio), 7 APP, 7 APP(pio)) served as non MWM controls. Two versions of the MWM, namely *spatial MWM* (8 WT, 7 WT(pio), 8 APP, 8 APP(pio)) and *non-spatial MWM* (8WT, 8 WT(pio), 7 APP, 7 APP(pio)), that differ with respect to cognitive demand (Lerch et al., 2011a) were used.

2.4.1. Spatial MWM

In the *spatial MWM*, a circular escape platform (10 cm diameter) was submerged 0.5 cm below the water surface in a fixed quadrant (target quadrant), and distal visual cues were available to the mice during the entire length of the protocol.

2.4.2. Non-spatial MWM

In the *non-spatial MWM*, the same platform was elevated above the water surface and marked by a visible cue (a cylinder 4 cm diameter × 4 cm, sitting on top of the platform). The cued platform was moved to a different location on each trial. A black curtain surrounded the pool, obscuring the distal visual landmarks, to minimize reliance on spatial strategies.

In both mazes, on each training day, mice received six training trials (presented in two blocks of three trials; inter-block interval was 1 h). The trial began by placing the mouse into the pool facing the wall, in one of four pseudo-randomly chosen start locations. The trial was complete once the mouse found the platform or 60 s had elapsed. If the mouse failed to find the platform on a given trial, the experimenter guided the mouse onto the platform. Spatial memory was assessed on day 5; 2 h after the final training trial, using a single 60 s probe trial during which the platform was removed from the pool. Movement of mice in the pool was followed and analyzed with the 2020 Plus tracking system and Water 2020 software (Ganz FC62D video camera; HVS Image). During training (learning phase of the test), we assessed the escape latency (the time to reach the platform) in both mazes over five days of training. In addition, for the *spatial MWM*, we assessed the swim path distance versus time and the mouse learning capacity using the slopes of the curves of the escape latencies (Drouin et al., 2011), which quantify the improvement of escape latency over time as a measure of learning. Performance in the *spatial MWM* probe trial was evaluated using crossings over the platform area (an index of memory precision; Morris, 1984), percent distance covered in the target quadrant (an index of memory retrieval; Morris, 1984), percent distance covered in non-target quadrants, and swim paths. Swim speed was evaluated both during training and probe trial.

2.5. Magnetic resonance imaging (MRI)

2.5.1. MRI sample preparation

In order to maximize our power to detect learning-related volume changes in these mice, we acquired high quality images post mortem with a resolution and contrast not obtainable in vivo (Lerch et al., 2012). Ten days post-MWM-training, mice were anaesthetized (65 mg/kg sodium pentobarbital, intra-peritoneal (i.p.)) and transcardially perfused with phosphate buffered saline (PBS, 30 ml, pH 7.4, 25 °C) followed by paraformaldehyde (4% PFA, 30 ml, 25 °C) plus 2 mM ProHance in PBS. Bodies, along with the skin, lower jaw, ears, and the cartilaginous nose tip were removed. The remaining skull structures containing the brain were allowed to postfix in 4% PFA plus 2 mM ProHance at 4 °C for 12 h. The skulls were then transferred to solution containing PBS, 0.02% sodium azide and 2 mM ProHance for 4 days at 15 °C. Mice serving as non MWM controls were subjected contemporaneously to the same procedure.

2.5.2. MRI acquisition

A multi-channel 7.0 Tesla MRI scanner (Varian Inc., Palo Alto, CA) with a 6-cm inner bore diameter insert gradient was used to acquire anatomical images of brains within skulls. Prior to imaging, the samples were removed from the contrast agent solution, blotted and placed into plastic tubes (13 mm diameter) filled with a proton-free susceptibility-matching fluid (Fluorinert FC-77, 3M Corp., St. Paul, MN). Three custom-built, solenoid coils (14 mm diameter, 18.3 cm in length) with over wound ends were used to image three brains in parallel. Parameters used in the scans were optimized for grey/white matter contrast (Lerch et al., 2011a): a T2-weighted, 3D fast spin-echo sequence was acquired with 6 echoes, with TR/TE = 325/32 ms, four averages, field-of-view $14 \times 14 \times 25$ mm^3 and matrix size = $432 \times 432 \times 780$, giving an image with 32 μm isotropic voxels. Total imaging time was 11.3 h per scan. The resulting images underwent a non-linear deformation algorithm (Avants et al., 2008) to align, in a blinded manner, corresponding anatomical features among all 103 brain images. This algorithm proceeded iteratively, aligning the individual images to an evolving average image that gained anatomical fidelity as more degrees of freedom were added to account for the individual anatomical differences. The final deformation fields that aligned each individual scan to the average were then analyzed using the Jacobian determinant to compute local volume change (Lerch et al., 2011b) for each mouse. Cortical thickness was also measured using a Laplacian thickness algorithm (Lerch et al., 2008). In addition to the voxel-wise analyses, an anatomical atlas comprised of 62 defined regions (Dorr et al., 2008) was used to perform automated template-based segmentation of regional volumes such that the same labeled template was applied to each scan (Collins et al., 1995). Using previously published guidelines (Dorr et al., 2008), this template was augmented to 64 defined regions by manual segmentation of hippocampus proper into the CA1, CA2, and CA3 subfields by a single investigator (A.B.) using the average volume generated from 103 independent mouse brain images. The software Display was used for manual segmentation (http://www.bic.mni.mcgill.ca/ServicesSoftwareVisualization/HomePage, MNI, Montréal, Canada). The guidelines for the location and boundaries of CA fields were obtained using the Mouse Allen Reference Atlas available online at http://www.brain-map.org/, The Mouse Brain in Stereotaxic Coordinates (Paxinos and Franklin, 2001), and CA pyramidal cell density gradient in a manner similar to published recommendations by Richards et al. (2011).

2.5.3. MRI data analysis

Statistics were performed separately on regional volumes as well as log Jacobians at every voxel. In each case, we used a heteroscedastic linear model, implemented using generalized least squares in the *NLME* package in R (Pinheiro and Bates, 2000), allowing for different variances per genotype. The linear model employed consisted of all main effects and interactions between the factors genotype (APP vs WT), treatment (pioglitazone vs. non-medicated), and maze training (spatial vs non-spatial). Multiple comparisons were corrected for using the False Discovery Rate (Genovese et al., 2002).

2.6. Histochemistry and quantification of staining

Following MR imaging, the fixed brains were removed from the skull and paraffin embedded. Coronal sections (5 μm-thick, 3 sections/mouse, 3–4 mice/group) taken through the hippocampus underwent Nissl (5 min in cresyl violet)- or thioflavine S (1% solution for 8 min)-staining. Nissl staining using cresyl violet stains the cell body, in particular nucleic acids in the cytoplasm, of the neurons blue, and is classically used to study neuronal cytoarchitectonics (Thompson, 2000). Thioflavine S binds to proteins with a β-pleated sheet conformation and is a well-established marker of amyloid plaques in the brain (Elghetany and Saleem, 1988). Sections were observed under a Leitz Aristoplan light microscope equipped with epifluorescence using an FITC filter (Leica). Pictures were acquired with a digital camera (Coolpix 4500; Nikon) and analyzed with the MetaMorph 6.1r3 software (Universal Imaging). Images were manually thresholded and areas of interest (midline and lateral parts of the CA1 region of the hippocampus) demarcated using fixed-area rectangular boxes (Nissl staining at 10× zoom) or the hippocampus proper (thioflavin S) were outlined in low power images (4× zoom). Per section, the average neuron size was calculated from ten randomly outlined neuronal cell bodies. In order to minimize the drift in the criteria used to manually outline the neurons we conducted the entire analyses in one sitting. The ratio of the area occupied by the Nissl-stained neurons in each area, along with the average cell size for each region, was used to calculate the average number of cells per CA1 subregion using the defined and constant surface area of the box outline. The area occupied by thioflavine S-positive parenchymal plaques was quantified as the percent surface area occupied in the delineated hippocampus.

2.7. Statistical analyses

The investigator was blinded for the LDF, non-spatial and spatial MWM, and histochemistry procedure and analyses. Statistical comparisons of LDF, MWM (non-spatial and spatial), and histochemistry (Nissl staining) data from 6-month-old mice were analyzed by two-way ANOVA followed by Newman–Keuls post hoc multiple comparison test (STATISTICA 10), with the exception of thioflavin S-stained hippocampal Aβ plaque load between APP and pioglitazone-treated APP mice that was compared using Student's *t* test (GraphPad Prism 4). Statistical comparison of LDF data from non-medicated 3-month-old WT and APP mice was analyzed by Student's *t* test for two-group (unpaired, Bonferroni-corrected), while LDF data post 3 days of pioglitazone-treatment was analyzed by Student's *t* test for within-group (paired) comparisons (GraphPad Prism 4). For all comparisons, a $p < 0.05$ was considered significant.

3. Results

3.1. Neural activity-evoked CBF in APP and WT mice: genotype and drug effects

Neural activity-evoked CBF response provides an index of neurovascular coupling. The CBF response evoked by whisker stimulation in the somatosensory cortex was significantly decreased in young APP mice, as compared to WT littermates (21.2 ± 0.4% vs 29.3 ± 0.9%, $p < 0.05$) (Fig. 1A,B), and persisted with age (17.7 ± 1.8% vs 26.8 ± 1.8%, $p < 0.01$) (Fig. 1C). Average percent flow deficit measured in APP mice was 27.8% at 3-months of age, and 34.2% at 6-months of age (Fig. 1B,C). Pioglitazone-treatment fully normalized this response with as little as 3-days of treatment (Fig. 1B), an effect that was maintained with long-term treatment (Fig. 1C). A small, but non-significant, enhancing effect on the average percent flow increase was observed in WT-treated mice (Fig. 1C).

3.2. Learning and memory in APP and WT mice

3.2.1. Genotype effect

In the *non-spatial MWM* task (visible platform, Fig. 2A), aside from small but significant punctual differences at days 1 and 4, the progressive decrease in escape latency over the five-day training period was comparable between WT and APP mice, thus ruling out overt visual, motor, and motivational deficits in APP mice. Mice displayed shorter escape latency in the *non-spatial MWM* compared to the *spatial MWM* (Fig. 2B), confirming the challenging nature of the latter despite similar sensorimotor and motivational requirements in both versions of the MWM (Lerch et al., 2011a). In the *spatial MWM* task, progressive decrease in escape latency (Fig. 2B), and distance swam prior to locating the hidden platform (Fig. 2D) over the five-day training period were significantly different ($p < 0.01$) between the two genotypes, indicating

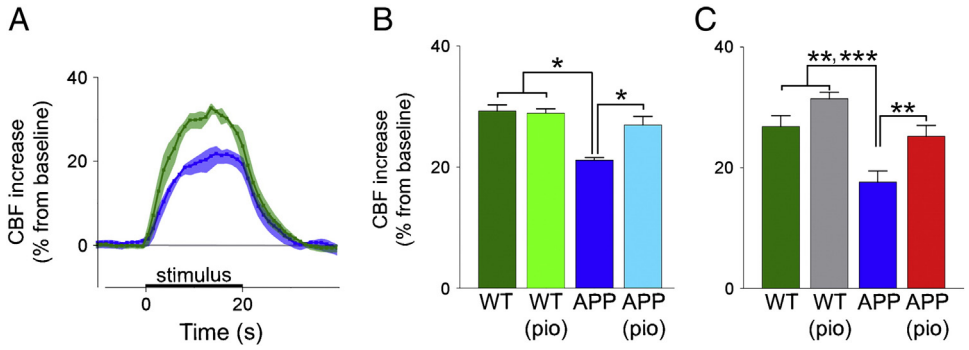

Fig. 1. Activity-induced CBF deficits in APP mice are normalized by pioglitazone. CBF changes were measured in the somatosensory cortex before and during whisker stimulation using laser Doppler flowmetry in 3-month and 6-month-old mice. Activity-induced CBF increase in 3-month-old APP mice (■, n = 5) was reduced compared to WT mice (■, n = 8), shown using (A) average LDF tracings for the entire 20 second stimulation period, and (B) overall means of the maximal percent change of CBF from baseline. Statistical analysis used was an unpaired two-tailed *t*-test (Bonferroni corrected). After 3 days of pioglitazone-treatment, the evoked CBF response measured in the same APP mice (■) was normalized completely, and remained unchanged in the WT mice (■). Statistical analysis used was a paired two-tailed *t*-test. (C) Compared to untreated WT mice (■, n = 5), the deficit in the activity-induced CBF response was present in 6-month-old untreated APP mice (■, n = 5). The activity-induced CBF response in 6-month-old APP mice (■, n = 4) treated for 3 months with pioglitazone did not differ from untreated and treated WT mice (■, n = 5), as shown using a two-way ANOVA. *p < 0.05, **p < 0.01, ***p < 0.001. Shaded area on line tracings in (A) define the SEM at each point. Error bars: SEM, CBF: cerebral blood flow, pio: pioglitazone, WT: wild-type.

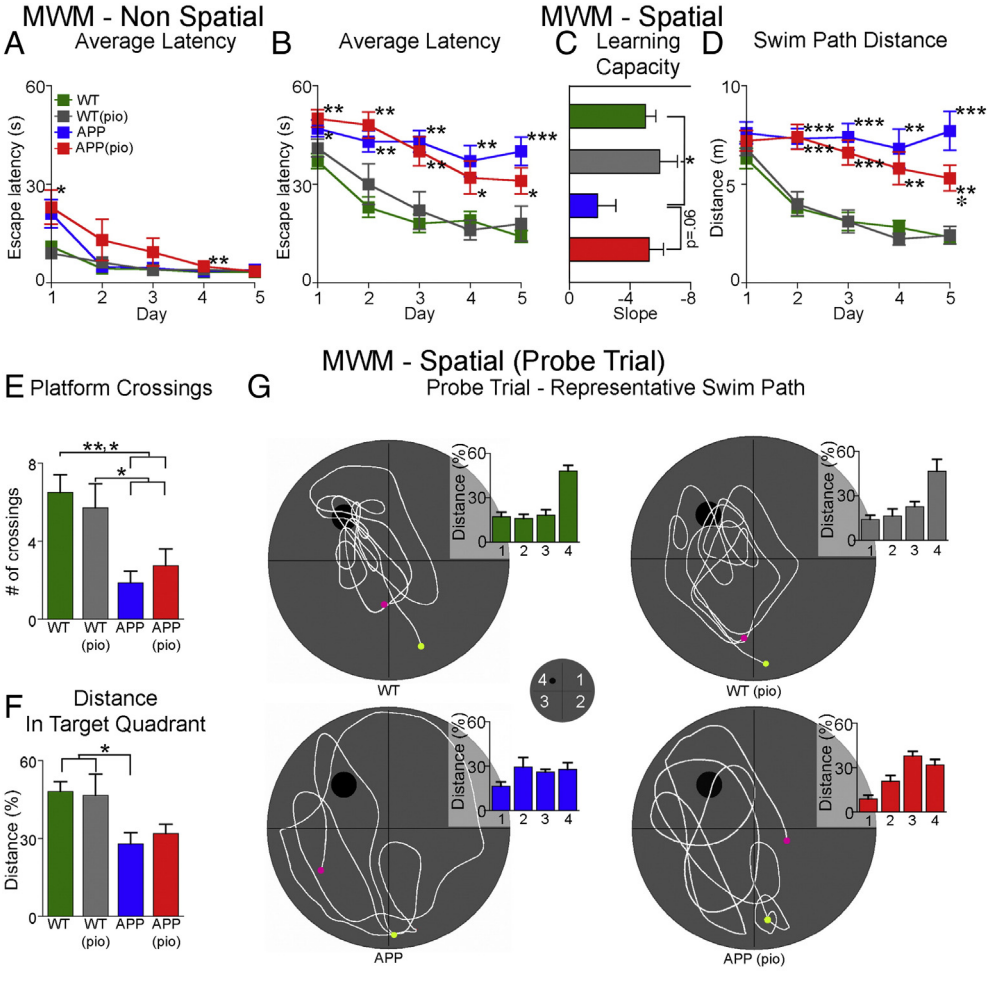

Fig. 2. Spatial learning and memory deficits in APP mice. (A) All mice undergoing non-spatial Morris water maze performed equally well at the end of training. (B) In contrast, 6-month-old APP mice (■) were impaired in the spatial Morris water maze, featuring significantly longer escape latencies in finding the hidden platform relative to WT controls (■). Pioglitazone slightly, but not significantly, improved learning performance in treated APP mice (■). (C) Compared to WT mice, learning capacity while impaired in APP mice was similar in pioglitazone-treated APP mice. (D) A decrease in the average distance swam per training day was observed in pioglitazone-treated APP mice compared to untreated APP mice, reaching significance on day 5. (E) In the probe trial, the number of crossings was slightly higher in pioglitazone-treated APP mice compared to APP mice, but still significantly different from WT mice. (F) Compared to WT mice, distance travelled in the correct quadrant was significantly lower in APP, but not in pioglitazone-treated APP mice. (G) Representative swim paths (● start, ● end) and percent distance travelled in each quadrant. Pioglitazone-treated APP mice showed mild improvement in the swim strategy used to locate the hidden platform. Overall, all groups displayed comparable swim speeds ruling out motor disabilities. Statistical analysis used was a two-way ANOVA. *p < .05 compared to APP, *p < .05, **p < .01, and ***p < .001 compared to WT. Pioglitazone-treated WT mice (■), error bars: SEM, pio: pioglitazone, WT: wild-type.

that APP mice have difficulty learning the spatial task. This was further evidenced by significantly ($p < 0.05$) diminished learning capacity in these mice over the five-day training period (slope $= -1.82 \pm 1.23$) compared to WT mice (slope $= -5.02 \pm 0.69$) (Fig. 2C). Moreover, in the probe trial, crossings at the target location (Fig. 2E), and the percent distance travelled in the target quadrant (Fig. 2F) by APP mice were significantly less ($p < 0.01$ and $p < 0.05$, respectively) than WT controls, consistent with reported deficits in memory retrieval and precision in these mice. These findings were not due to differences in swim speed, which was comparable amongst all groups (data not shown).

3.2.2. Drug effect

Pioglitazone had no effect in WT mice on *non-spatial* and *spatial MWM* as well as in the probe trial (Fig. 2). In the *spatial MWM*, a progressive decrease in average escape latency following blocks of training trials was observed in pioglitazone-treated, but not in untreated APP mice (Fig. 2B). This was confirmed by analysis of the learning capacity in pioglitazone-treated APP mice (slope $= -5.28 \pm 0.94$), which was improved to WT capacity (Fig. 2C). Accordingly, a decrease in the average distance swam per training day was observed in pioglitazone-treated, but not in untreated APP mice, reaching significance on day 5 ($p < 0.01$, Fig. 2D). Overall, the spatial training findings demonstrate that pioglitazone slightly improves spatial learning in APP mice. In the probe trial, pioglitazone-treated APP mice performed better than untreated APP mice in the number of platform crossings, but this measure failed to reach significance (Fig. 2E). The percent distance travelled in the target quadrant by pioglitazone-treated APP mice was not significantly different from WT controls (Fig. 2F). Interestingly, percent distance travelled in quadrant 3 (Fig. 2G) was significantly greater in treated compared to untreated APP mice ($p < 0.01$). This was reflective of the swim path used by pioglitazone-treated APP mice, which was largely restricted to quadrant 3 and the target quadrant, a finding that contrasted with the ineffective routes swam by untreated APP mice (Fig. 2G). Overall, the probe-trial findings show that pioglitazone exerts a mild beneficial effect on spatial memory-recall in APP mice.

3.3. Neuroanatomical differences in naïve APP and WT mice

3.3.1. Genotype effect

3.3.1.1. Region of interest (ROI) or brain substructure-based volume analyses. At 6-months of age, the average overall brain volume was 3.2% larger in APP mice (458.0 ± 18.5 mm^3) compared to age-matched WT controls (443.1 ± 12.1 mm^3, $p < 0.0001$). Volumetric analyses of 64 segmented brain structures revealed that 6 of 64 (9.3%) structures were significantly smaller, while the majority, i.e. 35 of 64 (54.7%) were significantly larger in APP mice compared to WT controls (Fig. 3). The greatest percent volume decrease (4.3%) in APP mice was in the habenular commissure, whereas the greatest increase (13.3%) was in the amygdala. Significant volume decreases were also observed in the interpeduncular nucleus, superior olivary complex, mammillary bodies, corticospinal tract pyramids, and cerebellar cortex. Interestingly, volumes of hippocampal regions including dentate gyrus, CA1, CA2, and CA3, as well as cortical structures involved in memory processing such as the entorhinal, temporoparietal, and frontal cortices were larger in APP mice.

3.3.1.2. Deformation based morphometry (DBM) — local volumetric analyses. Voxel-wise analysis provides a measure of local volumetric expansion (>0) or contraction (<0) relative to the reference space. A key feature of this approach is that it can detect small focal volume differences that may not be picked up in brain substructure-based approaches. Fig. 4C illustrates the differences found between APP and WT mice, with the red color scale indicating degrees of volume expansion, and the blue scale indicating degrees of volume contraction. Broad areas of volume expansion can be seen, in line with the overall

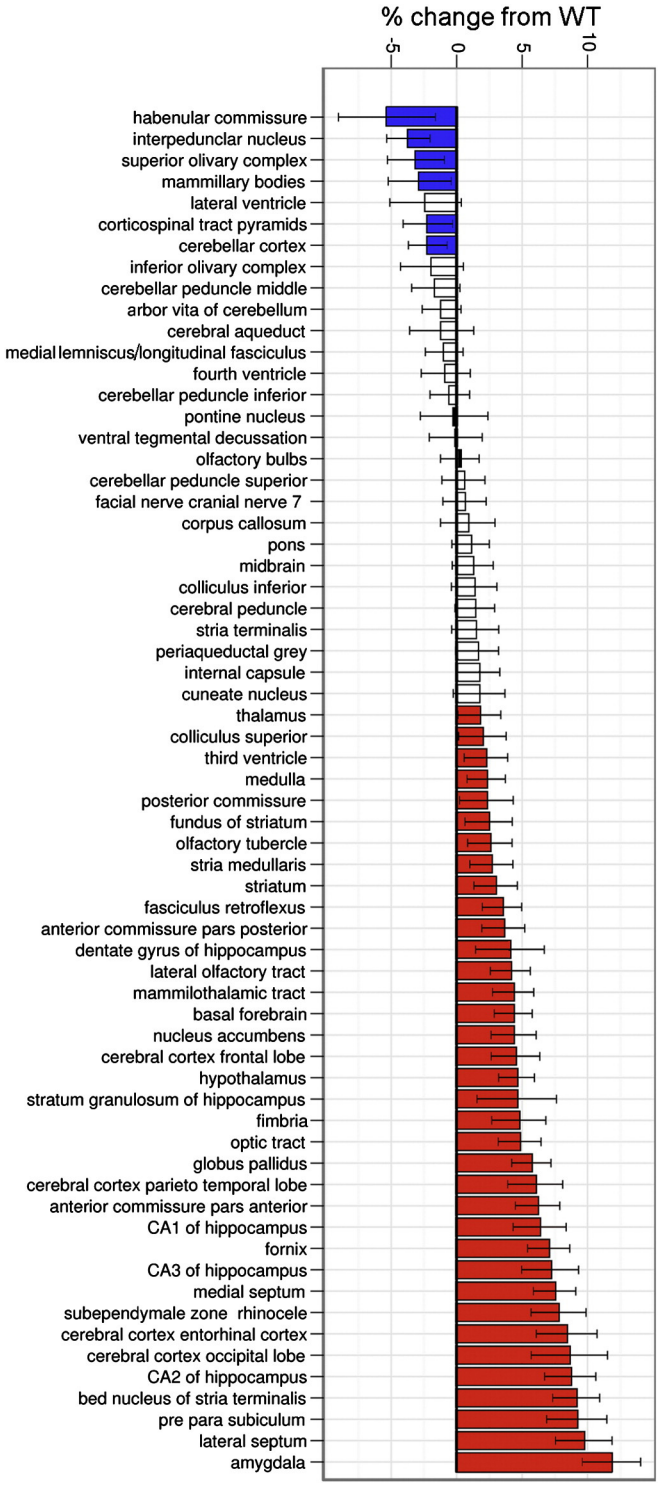

Fig. 3. Brain volume was overall increased in APP mice compared to WT. Percent change in volume of the 64 segmented brain structures in APP mice compared to WT controls. (□) q-value > 0.05, no change from WT; (■) q-value < 0.05, volume decrease from WT; (■) q-value < 0.05, volume increase from WT. Error bars: 95% confidence interval, WT: wild-type.

larger brains seen in the APP mice. Focal regions of volume contraction in APP relative to WT were found in corpus callosum and cingulum bundle, hippocampus (in particular, CA1 region adjacent to the midline, and CA3) and cerebellar cortex. It should be noted that while volume decrease in CA1 spanned almost the entire hippocampal septotemporal axis, in CA3 it was limited to the intermediate portion. Volume contraction in the corpus callosum and hippocampal CA1 subfield in APP mice

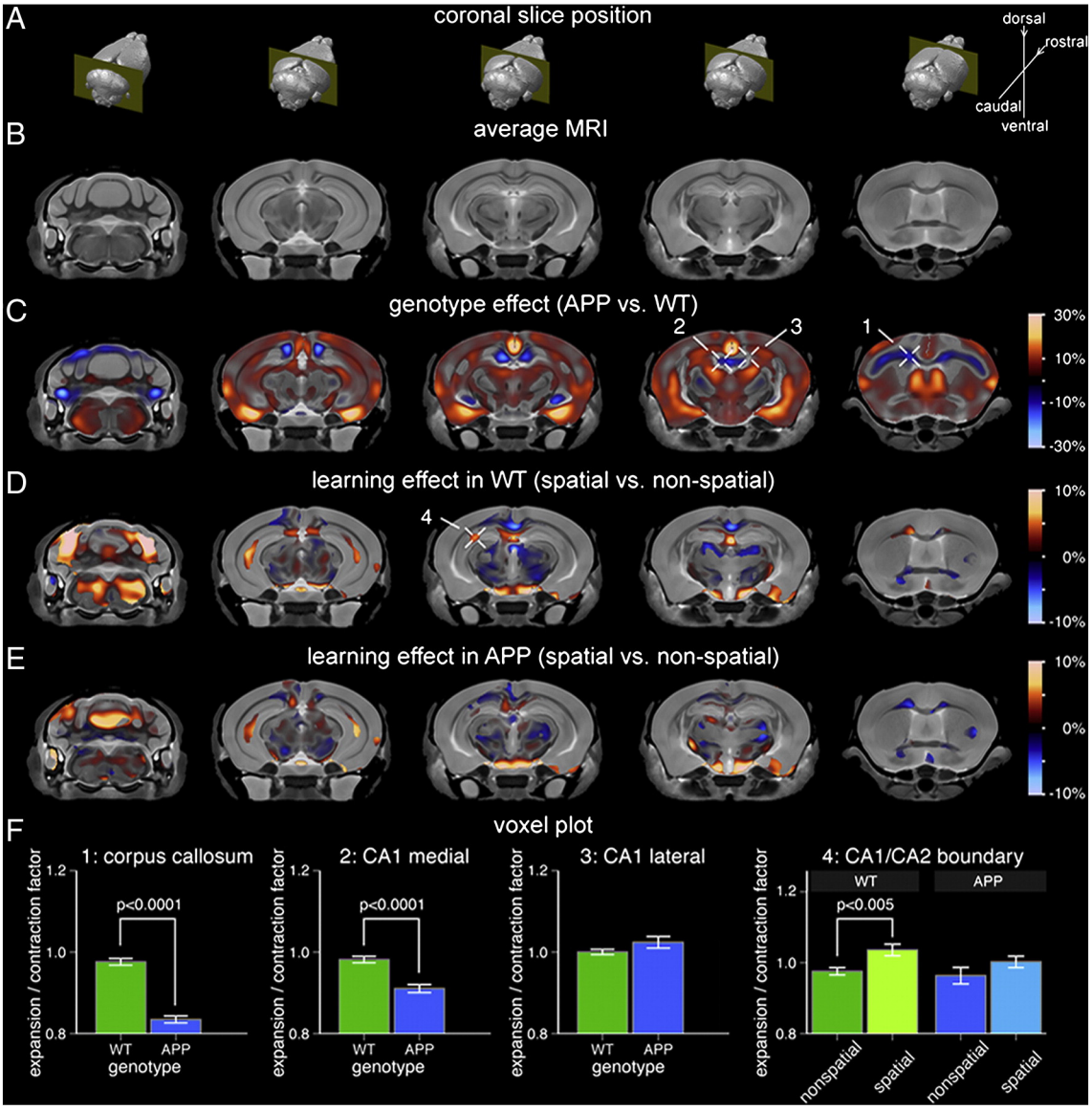

Fig. 4. Focal hippocampal volume increase associated with spatial learning and memory in WT mice is attenuated in APP mice. (A) Location of the five MRI slices shown in reference to the 3D brain. (B) Population-specific 3D MRI brain atlas. (C) Effect of genotype on local brain volume. Warm colors correspond to regions where APP brains were larger than WT whereas cool colors indicate regions that were smaller. The expansion/contraction map is masked based on statistical significance at a false discovery rate (FDR) of 10%. Cross-hairs 1 and 2 point to specific areas that are smaller in APP brains compared to WT, namely, the corpus callosum/cingulum bundle and the midline-adjacent CA1 regions, respectively. Cross-hair 3 points to an area of no change, specifically, the lateral CA1 region. (D) Expansion/contraction associated with spatial vs. non-spatial learning and memory in WT mice (masked at 10% FDR). Cross-hair 4 points to volume increase in the CA1/CA2 boundary region. (E) Expansion/contraction associated with spatial vs. non-spatial learning and memory in APP mice (same significance mask as in (D)). Compared to WT mice, APP mice display attenuated hippocampal volume increase following spatial Morris Water Maze performance. (F) The bar graphs show mean and standard error for the expansion/contraction factor associated with each selected voxel (cross-hairs c1–3 and d4). The genotype plots (1–3) have been normalized such that the WT homecage controls have a factor of 1.0. The training effect plots (4) have been normalized such that the homecage controls for respective genotypes have a factor of 1.0. WT: wild-type.

was further validated using voxel plots (Fig. 4F). In order to understand the cellular basis of the volume differences in the hippocampus, we performed histology on sections of the CA1 subfield.

3.3.1.3. Histochemical analyses. Qualitatively, Nissl-stained sections revealed irregular spreading of the CA1 pyramidal cells adjacent to the midline into the stratum oriens in 6-month-old APP mice (Fig. 5A). In contrast, there was a sharp demarcation between the CA1 pyramidal cell layer and stratum oriens in WT mice (Fig. 5A). Quantitatively, the percent area of the ROI occupied by cell bodies, and the average number of cells, were significantly reduced ($p < 0.05$) in APP mice (18.2 ± 2.4% and 188.1 ± 22.1, respectively) compared to WT controls (28.8 ± 0.4% and 329.5 ± 33.4, respectively) (Fig. 5B, C). The average cell size did not differ between APP (198.9 ± 5.0 μm^2) and WT (183.1 ± 15.2 μm^2) mice. As a negative control, we performed similar histochemical analyses on the lateral region of the CA1, which did not exhibit focal volume decrease (Fig. 4C,F), and found no qualitative (Fig. 5D) nor quantitative differences (Fig. 5E, F) between APP and WT mice.

3.3.1.4. Whole brain cortical thickness analyses. 6-month-old APP and WT mice exhibited differences in regional cortical thickness. In comparison to 6-month-old WT mice, increase in cortical thickness was observed in the frontal association areas, anterior cingulate, retrosplenial, entorhinal, perirhinal, and primary visual cortices of 6-month-old APP mice (Fig. 6A). The greatest percent cortical thickness increase in APP mice was in the lateral part of the entorhinal cortex (+15.6%; means,

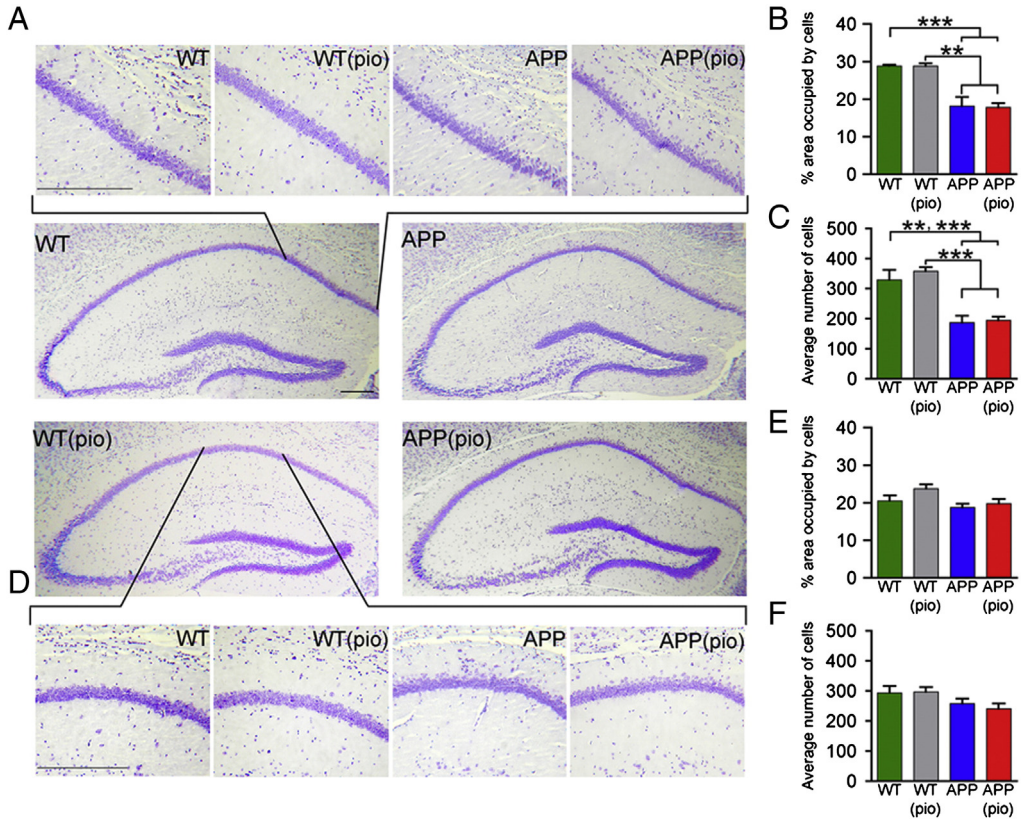

Fig. 5. Alterations in midline-adjacent CA1 area of the hippocampus in APP mice. (A) Nissl-stained hippocampal sections reveal disorganization of cells in the midline-adjacent CA1 pyramidal layer in 6-month-old APP mice. (B) Compared to age matched control (■) and pioglitazone-treated (■) WT mice, the area occupied by cell bodies is significantly reduced in control (■) and pioglitazone-treated (■) APP mice. (C) Similarly, irrespective of pioglitazone-treatment status, the average number of cells is significantly lower in APP mice compared to WT mice. (D) No qualitative difference was observed in the lateral CA1 region between 6-month-old APP and WT mice. Quantitatively, (E) the area occupied by cell bodies in the lateral CA1 region, and (F) the average numbers of cells were not significantly different between APP and WT mice. Statistical analysis used was a two-way ANOVA. Scale bars: 1 mm (low magnification images), 0.05 mm (high magnification images). **p < .01, ***p < .001. Error bars: SEM, pio: pioglitazone, WT: wild-type.

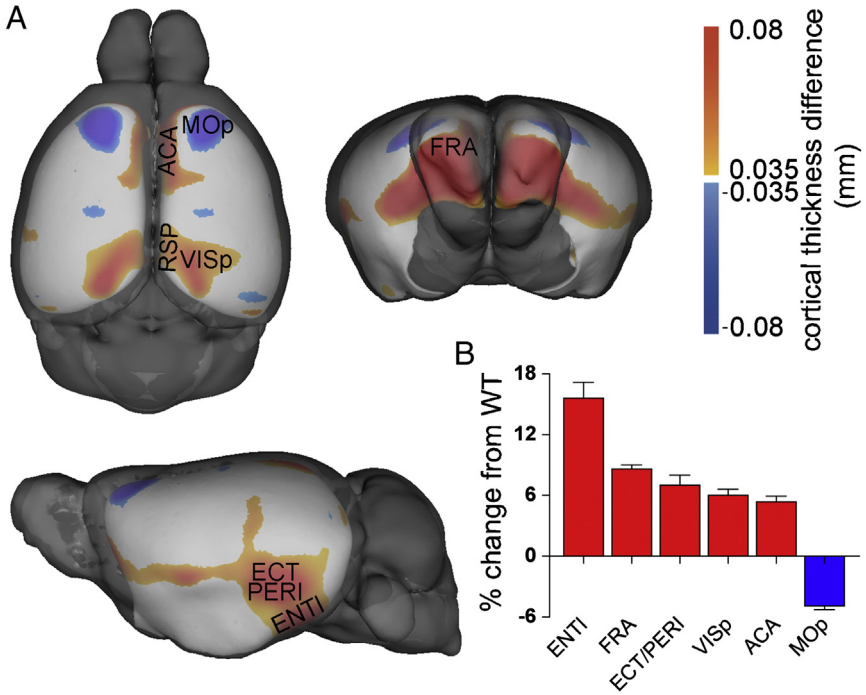

Fig. 6. Cortical thickness differences by genotype. (A) F-Statistic maps were thresholded at a false discovery rate of 5%. **Red** is APP > WT, **blue** is WT > APP. Thickness differences max out at 0.1 mm. (B) Percent change in cortical thickness of six regions in APP mice compared to WT controls. ENTl: entorhinal cortex (lateral part), FRA: frontal association cortex, ECT/PERI: ectorhinal/perirhinal cortex, VISp: primary visual cortex, ACA: anterior cingulate cortex, MOp: primary motor cortex, RSP: retrosplenial cortex, WT: wild-type. Brain structure abbreviations used are from the Mouse Allen Reference Atlas available online at http://www.brain-map.org.

0.64 ± 0.003 mm WT and 0.74 ± 0.007 mm APP), followed by the frontal association areas (+8.6%; means, 1.16 ± 0.004 mm WT and 1.26 ± 0.007 mm APP), while a reduction (−4.9%; means, 1.42 ± 0.004 mm WT and 1.35 ± 0.006 mm APP) was seen in the primary motor cortex of APP mice (Fig. 6B).

3.3.2. Drug effect

No significant differences in the volume of brain structures or cortical thickness were detected in pioglitazone-treated APP and WT mice compared to their respective untreated controls. In line with the overall lack of treatment-effect on brain structure volumes, Nissl-staining did not detect any qualitative (Fig. 5A, D) nor significant quantitative (Fig. 5B, C, E, F) differences in the hippocampal CA1 subfield between pioglitazone-treated APP and WT mice compared to their respective untreated controls. Moreover, consistent with no treatment effect on brain volume and with earlier findings in old APP mice (Nicolakakis et al., 2008), there was also no difference in the Aβ plaque load in the hippocampus between pioglitazone-treated and untreated APP mice (Fig. 7).

3.4. Brain volume differences between spatial and non-spatial MWM

3.4.1. Genotype effect

To test whether the response to spatial training differed by genotype, we computed separate voxel-wise linear models relating local brain volume to *MWM* (i.e. *spatial* vs. *non-spatial*). DBM analyses of WT mice that had performed the *spatial MWM* compared to those that performed the *non-spatial MWM* revealed significant focal volume increase (6%) in a contiguous region of the hippocampus beginning rostrally at the CA1/CA2 boundary region and extending caudally along both CA1 and CA2 (Fig. 4D). The increase in volume was lateralized to the left dorsal hippocampus. In comparison, for the same contrast in APP mice, focal volume increase in the CA1/CA2 boundary region was reduced (3.8%) relative to that seen in WT mice (Fig. 4E). The training effect remained significant in the WT mice, whereas the effects in the APP did not survive multiple comparison correction (Fig. 4F). Outside the hippocampus, significant focal volume increases were observed in the corpus callosum and cingulum bundle, entorhinal cortex, and the cerebellum of WT mice that had undergone the *spatial MWM* (Fig. 4D).

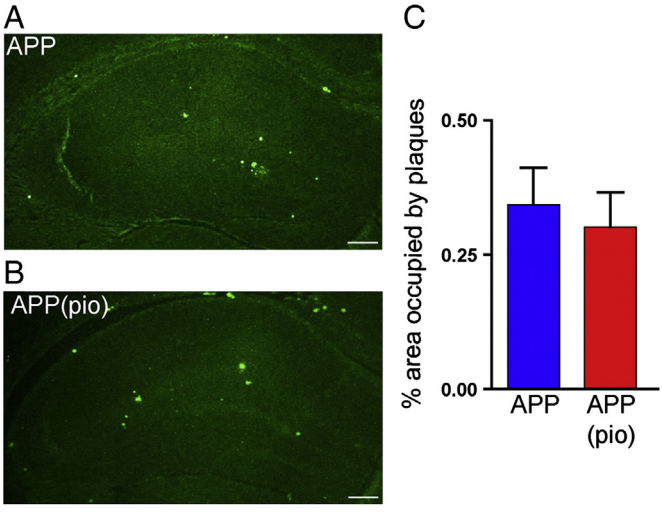

Fig. 7. Pioglitazone did not reduce Aβ plaque load in the hippocampus. Qualitatively, the area occupied by thioflavin S-stained mature, dense-core amyloid plaques in the hippocampus of 6-month-old (A) APP mice and (B) pioglitazone-treated APP (APP (pio)) mice were comparable. (C) Quantitatively, pioglitazone-treatment did not reduce amyloid plaque load. Scale bar: 1 mm (4× zoom), error bars: SEM, pio: pioglitazone.

3.4.2. Drug effect

No significant focal brain volume differences were observed in pioglitazone-treated WT or APP mice undergoing *spatial* versus *non-spatial MWM*.

4. Discussion

4.1. Mutated-hAPP overexpression induces neuroanatomical reshaping

4.1.1. Brain structure volume abnormalities

We find that brain volume is abnormal in 6-month-old APP mice, with both atrophy and hypertrophy present at the level of the brain substructures. Brain atrophy, both global and regional, is a hallmark feature of AD. Interestingly, the majority of atrophied structures identified in APP mice, namely the habenular commissure, interpeduncular nucleus, mammillary bodies, and cerebellar cortex are emerging extrahippocampal players in spatial memory processing (Bianco and Wilson, 2009; Kobayashi et al., 2013; Rochefort et al., 2013; Vann and Aggleton, 2003). Volume decreases in the latter two structures has also been reported in AD patients (Andersen et al., 2012; Copenhaver et al., 2006; Wegiel et al., 1999).

In contrast, the observation that the majority of brain-substructures, including the hippocampus, are hypertrophic in APP mice is unexpected, but has precedent. Similar observations of regional brain volume hypertrophy have been reported in pre-symptomatic familial AD mutation carriers (Fortea et al., 2010; Lee et al., 2013) and in 6-month-old $APP_{(Swe)}/PS1_{(M146V)}$ mice on the same C57BL/6J background as our mice (Maheswaran et al., 2009). Possible mechanisms accounting for regional brain volume increase in mouse models of familial AD include (a) the space-occupying effects of Aβ-deposits, and soluble/deposited Aβ-induced inflammatory response (e.g. gliosis and edema) in the absence of brain tissue loss (Fox et al., 2005; Maheswaran et al., 2009); (b) hAPP overexpression-induced increase in neurogenesis (Jin et al., 2004), and/or a shift in the distribution of neuronal cell size toward larger neurons (Oh et al., 2009); and (c) compensatory neuronal hypertrophy, an early cellular attempt at offsetting neuronal injury induced by Aβ (Driscoll and Troncoso, 2011). While the latter requires investigation in murine AD models, cortical and hippocampal neuronal hypertrophy has been demonstrated in asymptomatic AD cohorts from the Baltimore Longitudinal Study of Aging (O'Brien et al., 2009; Riudavets et al., 2007) and the Nun Study (Iacono et al., 2009).

The variability in global and regional brain volume differences reported in APP mouse models, ranging from atrophic (Badea et al., 2010; Lau et al., 2008; Redwine et al., 2003) to hypertrophic could be explained, in part, by variations in transgene(s) combination, promoter used for hAPP expression, the number and location of hAPP mutation(s), and genetic background. These variables impact APP expression, soluble and deposited Aβ-levels, and Aβ-related neuroinflammation and oxidative stress indices (Crews et al., 2010; Scahill et al., 2013). These factors, together with age, method and locus of measurement, likely explain the observed variability in mutated-hAPP overexpression-induced neuroanatomical reshaping.

4.1.2. Focal brain volume differences

Voxel-wise DBM analysis demonstrated broad areas of volume expansion and selective areas of contraction in the 6-month-old APP brain, generally consistent with the brain structure-level analysis. However, voxel-level analysis revealed small areas of focal volume decreases bilaterally within the otherwise hypertrophic hippocampal subfields CA1 and CA3, with atrophy more spatially extensive within CA1. Our finding in APP mice is consistent with the MRI-detectable sub-regional CA1 volume decreases apparent in early AD (Frisoni et al., 2008; Kerchner et al., 2010). Previous work from our group using the same analysis procedure to compare ex vivo and in vivo MRI data found good agreement in brain morphology, supporting the interpretation of the observed changes as focal volume changes rather than local effects of fixation (Lerch et al., 2012).

In order to understand the cellular basis of focal volume decrease in the hippocampal subfields of APP mice, we performed histopathology on the locus in CA1 and demonstrated significantly low cell counts and disorganization of pyramidal layer (CA1sp) neurons. Neuron loss in the CA1, in particular the CA1sp, has been documented in AD patients (Davies et al., 1992). Loss of septal CA1 neurons was recently found in 6-month-old J20 APP mice using ROI-based stereological methods (Wright et al., 2013). Our study extends this finding by demonstrating that at this age, neuron loss in the CA1, especially that in the CA1sp, is selective to medial CA1 and spans almost the entire hippocampal septotemporal axis. In summary, since both CA1 and CA3 neurons are critically involved in spatial learning/memory in rodents (Florian and Roullet, 2004; Maviel et al., 2004) and humans (Holden et al., 2012; Suthana et al., 2009), the mutated hAPP-specific localized hippocampal atrophy most likely contributes to impaired spatial MWM performance in our APP mice.

Outside the hippocampus, we demonstrated bilateral focal volume decreases within the cerebellar cortex, an extrahippocampal substrate for spatial cognition (Rochefort et al., 2013). Sub-regional volume decreases were also observed in the anterior part of the medial and lateral white matter (WM) tracts, specifically, the cingulum (CG) and underlying corpus callosum (CC). In rodents, CG and CC lesions impair spatial behaviour (Aggleton et al., 1995), including spatial MWM performance (Warburton et al., 1998). Volumetric reductions in CG (Villain et al., 2008) and CC (Di Paola et al., 2010) also occur in MCI and AD patients.

4.1.3. Aberrant cortical thickness

Using an automated algorithm to measure thickness across the entire cortex, we demonstrate that cortical thickness is aberrant in 6-month-old APP mice. Since APP is a crucial player in processes controlling cortical development (Herms et al., 2004) mutated-hAPP overexpression may be a factor in the abnormal cortical phenotype in APP mice. Cortical thickening was present in the entorhinal, perirhinal, retrosplenial, anterior cingulate, and frontal association cortices, all key neocortical structures involved in spatial learning/memory (Vann and Albasser, 2011). While unexpected in the AD literature, cortical thickening has been reported in middle-aged apolipoproteinEε4 individuals, negatively impacting their spatial-cueing (Espeseth et al., 2010), and pre-symptomatic familial AD presenilin-1 mutation carriers (Fortea et al., 2010). This group then observed an inverted U-shaped relationship between cortical thickness and CSF-Aβ42 levels, suggesting that pathological increases in cortical thickness may precede thinning as Aβ-plaques accumulate in the brain (Fortea et al., 2011). Recent in vivo work in J20 APP mice supports the idea of a temporal evolution of cortical thickness abnormalities, with aberrant thickening of the regions involved in spatial memory/learning occurring between 1 and 3 months of age (Grand'maison et al., 2013; Hebert et al., 2013). Our current results suggest that these same cortical regions remain abnormally thick at least until 6 months of age, when Aβ deposition and spatial memory deficits have just been established. The greater rate of cortical thinning evident in these mice by 12-months, compared to age-matched WT controls (Hebert et al., 2013), is reminiscent of the cortical thickness pattern observed in familial AD mutation carriers (Fortea et al., 2010) with a transitory thickening preceding thinning associated with disease progression.

4.2. Mutated-hAPP attenuates learning and memory-induced neuroanatomical plasticity

We found that in 6-month-old WT mice, successful spatial learning/retrieval induced robust volume increases within the hippocampus. These increases were localized to a contiguous region beginning rostrally at the CA1/CA2 boundary-region and extending caudally along CA1 and CA2, consistent with the effect of spatial MWM on dorsal hippocampal volume that we observed in 3-month-old WT mice (Lerch et al., 2011a). The magnitude of this increase was greatly reduced in the CA1/CA2 boundary-region of age-matched APP mice, a finding consistent with their poor spatial MWM performance. Three lines of evidence support our MRI-based neuroanatomical plasticity findings in WT mice. Lesion-based research in rats shows that dorsal, but not ventral, hippocampal lesions impair acquisition on the spatial MWM (Moser et al., 1995). Enhanced metabolic activity in rostral CA1, extending caudally, has been demonstrated in mice following spatial radial arm maze (Ros et al., 2006). Electrophysiological studies have shown that the dorsal hippocampus houses a higher proportion of place cells (cells responding to spatial information), and focused place fields compared to its ventral counterpart (Jung et al., 1994). Our finding of left-lateralization of volume increase in the CA1/CA2 boundary-region is further supported by studies demonstrating that left, but not right, hippocampus inactivation prior to spatial MWM training weakened rodent probe-trial performance (Klur et al., 2009), and that virtual-spatial MWM learning in human increased left-anterior hippocampal activity (Cornwell et al., 2008). Since, these findings suggest that the left hippocampus facilitates spatial memory encoding/consolidation and the right aids memory-retrieval, it appears that attenuated hippocampal plasticity in APP mice perturbs the former process.

4.3. Effect of pioglitazone-treatment

4.3.1. Pioglitazone abrogates mutated-hAPP-induced cerebrovascular dysfunction

We show that neuronal activity-evoked CBF response in the somatosensory area of the neocortex was impaired in young APP mice prior to amyloid plaque deposition (Mucke et al., 2000) and measurable mnemonic impairment (DeIpolyi et al., 2008), and persisted into adulthood. We demonstrate that pioglitazone counters this chronic cerebrovascular insufficiency as early as 3 days into treatment. This study extends our previous findings of beneficial effects of short-term pioglitazone-treatment on stimulus-induced increases in cerebral perfusion and glucose metabolism, and cerebrovascular reactivity in aged APP mice (Nicolakakis et al., 2008). Together, the results confirm that cerebrovascular insufficiency, in particular reduced baseline (Hebert et al., 2013; Niwa et al., 2002) and stimulus-evoked CBF (Niwa et al., 2000), is an early pathogenic marker found in various APP mouse models of AD. Our study also indicates that pioglitazone is a potent reverser of cerebrovascular dysfunction at all stages of Aβ-induced pathology in APP mice. It thus has the potential to alleviate the chronic cerebrovascular insufficiency observed in AD (Chen et al., 2011; Iadecola, 2004; Rodriguez et al., 2000; Zlokovic et al., 2005). Supporting our hypothesis is the finding that daily pioglitazone intake for 6 months improves parietal lobe CBF in mild AD patients with T2DM (Sato et al., 2009).

4.3.2. Pioglitazone exerts beneficial effects on spatial learning and memory

We found that long-term pioglitazone-treatment commencing in young APP mice improved spatial learning capacity to WT levels, and exerted a mild positive effect on memory recall in adult APP mice. The beneficial effect on cognition may be due to the combined ability of pioglitazone to sustainably abrogate cerebrovascular dysfunction starting in young mice and, as previously demonstrated, reduce indexes of neuronal dysfunction such as cerebral oxidative stress, glial activation, and cholinergic denervation (Nicolakakis et al., 2008). However, it is also possible that the limited benefits of pioglitazone on cognitive function occur independently from the CBF improvements. In the AD literature to date, pioglitazone has been shown to improve regional CBF and cognitive function in mild AD patients with T2DM (Sato et al., 2009), and has been recommended for testing in earlier disease stages of AD (Geldmacher et al., 2011). A clinical trial testing the ability of a low dose of pioglitazone to delay the onset of MCI of the AD type is expected to launch this year (Crenshaw et al., 2013).

Pioglitazone treatment did not improve learning/memory-induced neuroanatomical plasticity and hAPP-induced aberrant neuroanatomical reshaping, supporting the notion that the substrate for cognitive

deficits in AD is multifactorial, and treatment-paradigms may need to address multiple root causes to achieve the best outcomes.

5. Conclusions

In summary, overexpression of mutated-hAPP in mice induces aberrant neuroanatomical reshaping, cerebrovascular dysfunction, deficits in spatial learning/memory and associated neuroanatomical plasticity. Early, long-term intervention with pioglitazone rescues brain hemodynamics and exerts positive effects on spatial learning and memory. Since treatment of vascular risk factors and/or vascular co-morbidities has been shown to slow cognitive decline (Deschaintre et al., 2009; Li et al., 2011), pioglitazone may be of benefit to AD patients with concurrent cerebrovascular deficits. Absence of a corresponding recovery in neuroanatomical plasticity in treated APP mice with normalized functional hyperemia implicates impaired neuroanatomical plasticity as an additional factor contributing to cognitive deficits, possibly defining a new therapeutic target.

Author contributions

All authors contributed to the design of the experiments. A.B. performed experiments, analyzed data and prepared the manuscript. J.P.L processed the MRI data and analyzed the cortical thickness data. E.H. together with J.G.S. supervised the project and contributed to the writing of the manuscript. J.G.S provided statistical expertise for the neuroimaging analyses.

Acknowledgements

This study is supported by grants from the Canadian Institutes of Health Research (CIHR, MOP-84275, EH), Ontario Research Fund (ORF-RE, JS), and Takeda Pharmaceuticals U.S.A., Inc. (EH), and a CIHR Banting and Best Canada Graduate Scholarship (AB). We thank Dr. L. Mucke (Gladstone Inst. of Neurological Disease and Dept. Neurology, UCSF, CA, USA) and the J. David Gladstone Institutes for the APP transgenic mouse breeders, Ms. P. Fernandes (Montreal Neurological Institute) for the laser Doppler flowmetry experiments, and Dr. S. Narayanan (Montreal Neurological Institute) for comments on the manuscript.

References

Aggleton, J.P., Neave, N., Nagle, S., Sahgal, A., 1995. A comparison of the effects of medial prefrontal, cingulate cortex, and cingulum bundle lesions on tests of spatial memory: evidence of a double dissociation between frontal and cingulum bundle contributions. J. Neurosci. 15, 7270–7281.

Amieva, H., Jacqmin-Gadda, H., Orgogozo, J.M., Le Carret, N., Helmer, C., Letenneur, L., Barberger-Gateau, P., Fabrigoule, C., Dartigues, J.F., 2005. The 9 year cognitive decline before dementia of the Alzheimer type: a prospective population-based study. Brain 128, 1093–1101.

Andersen, K., Andersen, B.B., Pakkenberg, B., 2012. Stereological quantification of the cerebellum in patients with Alzheimer's disease. Neurobiol. Aging 33, 197 (e111-120).

Avants, B.B., Epstein, C.L., Grossman, M., Gee, J.C., 2008. Symmetric diffeomorphic image registration with cross-correlation: evaluating automated labeling of elderly and neurodegenerative brain. Med. Image Anal. 12, 26–41.

Badea, A., Johnson, G.A., Jankowsky, J.L., 2010. Remote sites of structural atrophy predict later amyloid formation in a mouse model of Alzheimer's disease. Neuroimage 50, 416–427.

Bianco, I.H., Wilson, S.W., 2009. The habenular nuclei: a conserved asymmetric relay station in the vertebrate brain. Philos. Trans. R. Soc. Lond. B Biol. Sci. 364, 1005–1020.

Chen, W., Song, X., Beyea, S., D'Arcy, R., Zhang, Y., Rockwood, K., 2011. Advances in perfusion magnetic resonance imaging in Alzheimer's disease. Alzheimers Dement. 7, 185–196.

Collins, D.L., Holmes, C.J., Peters, T.M., Evans, A.C., 1995. Automatic 3-D model-based neuroanatomical segmentation. Hum. Brain Mapp. 3, 190–208.

Copenhaver, B.R., Rabin, L.A., Saykin, A.J., Roth, R.M., Wishart, H.A., Flashman, L.A., Santulli, R.B., McHugh, T.L., Mamourian, A.C., 2006. The fornix and mammillary bodies in older adults with Alzheimer's disease, mild cognitive impairment, and cognitive complaints: a volumetric MRI study. Psychiatry Res. 147, 93–103.

Cornwell, B.R., Johnson, L.L., Holroyd, T., Carver, F.W., Grillon, C., 2008. Human hippocampal and parahippocampal theta during goal-directed spatial navigation predicts performance on a virtual Morris water maze. J. Neurosci. 28, 5983–5990.

Crenshaw, D.G., Gottschalk, W.K., Lutz, M.W., Grossman, I., Saunders, A.M., Burke, J.R., Welsh-Bohmer, K.A., Brannan, S.K., Burns, D.K., Roses, A.D., 2013. Using genetics to enable studies on the prevention of Alzheimer's disease. Clin. Pharmacol. Ther. 93, 177–185.

Crews, L., Rockenstein, E., Masliah, E., 2010. APP transgenic modeling of Alzheimer's disease: mechanisms of neurodegeneration and aberrant neurogenesis. Brain Struct. Funct. 214, 111–126.

Davies, D.C., Horwood, N., Isaacs, S.L., Mann, D.M., 1992. The effect of age and Alzheimer's disease on pyramidal neuron density in the individual fields of the hippocampal formation. Acta Neuropathol. 83, 510–517.

Delpolyi, A.R., Fang, S., Palop, J.J., Yu, G.Q., Wang, X., Mucke, L., 2008. Altered navigational strategy use and visuospatial deficits in hAPP transgenic mice. Neurobiol. Aging 29, 253–266.

Deschaintre, Y., Richard, F., Leys, D., Pasquier, F., 2009. Treatment of vascular risk factors is associated with slower decline in Alzheimer disease. Neurology 73, 674–680.

Di Paola, M., Luders, E., Di Iulio, F., Cherubini, A., Passafiume, D., Thompson, P.M., Caltagirone, C., Toga, A.W., Spalletta, G., 2010. Callosal atrophy in mild cognitive impairment and Alzheimer's disease: different effects in different stages. Neuroimage 49, 141–149.

Dorr, A.E., Lerch, J.P., Spring, S., Kabani, N., Henkelman, R.M., 2008. High resolution three-dimensional brain atlas using an average magnetic resonance image of 40 adult C57Bl/6J mice. Neuroimage 42, 60–69.

Draganski, B., Gaser, C., Busch, V., Schuierer, G., Bogdahn, U., May, A., 2004. Neuroplasticity: changes in grey matter induced by training. Nature 427, 311–312.

Driscoll, I., Troncoso, J., 2011. Asymptomatic Alzheimer's disease: a prodrome or a state of resilience? Curr. Alzheimer Res. 8, 330–335.

Drouin, A., Bolduc, V., Thorin-Trescases, N., Belanger, E., Fernandes, P., Baraghis, E., Lesage, F., Gillis, M.A., Villeneuve, L., Hamel, E., Ferland, G., Thorin, E., 2011. Catechin treatment improves cerebrovascular flow-mediated dilation and learning abilities in atherosclerotic mice. Am. J. Physiol. Heart Circ. Physiol. 300, H1032–H1043.

Elghetany, M.T., Saleem, A., 1988. Methods for staining amyloid in tissues: a review. Stain Technol. 63, 201–212.

Espeseth, T., Westlye, L.T., Walhovd, K.B., Fjell, A.M., Endestad, T., Rootwelt, H., Reinvang, I., 2010. Apolipoprotein E epsilon4-related thickening of the cerebral cortex modulates selective attention. Neurobiol. Aging 33, 304–322.

Florian, C., Roullet, P., 2004. Hippocampal CA3-region is crucial for acquisition and memory consolidation in Morris water maze task in mice. Behav. Brain Res. 154, 365–374.

Fortea, J., Sala-Llonch, R., Bartres-Faz, D., Bosch, B., Llado, A., Bargallo, N., Molinuevo, J.L., Sanchez-Valle, R., 2010. Increased cortical thickness and caudate volume precede atrophy in PSEN1 mutation carriers. J. Alzheimers Dis. 22, 909–922.

Fortea, J., Sala-Llonch, R., Bartres-Faz, D., Llado, A., Sole-Padulles, C., Bosch, B., Antonell, A., Olives, J., Sanchez-Valle, R., Molinuevo, J.L., Rami, L., 2011. Cognitively preserved subjects with transitional cerebrospinal fluid ss-amyloid 1–42 values have thicker cortex in Alzheimer's disease vulnerable areas. Biol. Psychiatry 70, 183–190.

Fox, N.C., Black, R.S., Gilman, S., Rossor, M.N., Griffith, S.G., Jenkins, L., Koller, M., 2005. Effects of Abeta immunization (AN1792) on MRI measures of cerebral volume in Alzheimer disease. Neurology 64, 1563–1572.

Frisoni, G.B., Ganzola, R., Canu, E., Rub, U., Pizzini, F.B., Alessandrini, F., Zoccatelli, G., Beltramello, A., Caltagirone, C., Thompson, P.M., 2008. Mapping local hippocampal changes in Alzheimer's disease and normal ageing with MRI at 3 Tesla. Brain 131, 3266–3276.

Geldmacher, D.S., Fritsch, T., McClendon, M.J., Landreth, G., 2011. A randomized pilot clinical trial of the safety of pioglitazone in treatment of patients with Alzheimer disease. Arch. Neurol. 68, 45–50.

Genovese, C.R., Lazar, N.A., Nichols, T., 2002. Thresholding of statistical maps in functional neuroimaging using the false discovery rate. Neuroimage 15, 870–878.

Grand'maison, M., Zehntner, S.P., Ho, M.K., Hebert, F., Wood, A., Carbonell, F., Zijdenbos, A.P., Hamel, E., Bedell, B.J., 2013. Early cortical thickness changes predict beta-amyloid deposition in a mouse model of Alzheimer's disease. Neurobiol. Dis. 54, 59–67.

Hebert, F., Grand'maison, M., Ho, M.K., Lerch, J.P., Hamel, E., Bedell, B.J., 2013. Cortical atrophy and hypoperfusion in a transgenic mouse model of Alzheimer's disease. Neurobiol. Aging 34, 1644–1652.

Henderson, V.W., Mack, W., Williams, B.W., 1989. Spatial disorientation in Alzheimer's disease. Arch. Neurol. 46, 391–394.

Herms, J., Anliker, B., Heber, S., Ring, S., Fuhrmann, M., Kretzschmar, H., Sisodia, S., Muller, U., 2004. Cortical dysplasia resembling human type 2 lissencephaly in mice lacking all three APP family members. EMBO J. 23, 4106–4115.

Holden, H.M., Hoebel, C., Loftis, K., Gilbert, P.E., 2012. Spatial pattern separation in cognitively normal young and older adults. Hippocampus 22, 1826–1832.

Iacono, D., Markesbery, W.R., Gross, M., Pletnikova, O., Rudow, G., Zandi, P., Troncoso, J.C., 2009. The Nun study: clinically silent AD, neuronal hypertrophy, and linguistic skills in early life. Neurology 73, 665–673.

Iadecola, C., 2004. Neurovascular regulation in the normal brain and in Alzheimer's disease. Nat. Rev. Neurosci. 5, 347–360.

Jin, K., Galvan, V., Xie, L., Mao, X.O., Gorostiza, O.F., Bredesen, D.E., Greenberg, D.A., 2004. Enhanced neurogenesis in Alzheimer's disease transgenic (PDGF-APPSw, Ind) mice. Proc. Natl. Acad. Sci. U. S. A. 101, 13363–13367.

Jung, M.W., Wiener, S.I., McNaughton, B.L., 1994. Comparison of spatial firing characteristics of units in dorsal and ventral hippocampus of the rat. J. Neurosci. 14, 7347–7356.

Kerchner, G.A., Hess, C.P., Hammond-Rosenbluth, K.E., Xu, D., Rabinovici, G.D., Kelley, D.A., Vigneron, D.B., Nelson, S.J., Miller, B.L., 2010. Hippocampal CA1 apical neuropil atrophy in mild Alzheimer disease visualized with 7-T MRI. Neurology 75, 1381–1387.

Klur, S., Muller, C., Pereira de Vasconcelos, A., Ballard, T., Lopez, J., Galani, R., Certa, U., Cassel, J.C., 2009. Hippocampal-dependent spatial memory functions might be lateralized in rats: an approach combining gene expression profiling and reversible inactivation. Hippocampus 19, 800–816.

Kobayashi, Y., Sano, Y., Vannoni, E., Goto, H., Suzuki, H., Oba, A., Kawasaki, H., Kanba, S., Lipp, H.P., Murphy, N.P., Wolfer, D.P., Itohara, S., 2013. Genetic dissection of medial habenula-interpeduncular nucleus pathway function in mice. Front. Behav. Neurosci. 7, 17.

Lau, J.C., Lerch, J.P., Sled, J.G., Henkelman, R.M., Evans, A.C., Bedell, B.J., 2008. Longitudinal neuroanatomical changes determined by deformation-based morphometry in a mouse model of Alzheimer's disease. Neuroimage 42, 19–27.

Lee, G.J., Lu, P.H., Medina, L.D., Rodriguez-Agudelo, Y., Melchor, S., Coppola, G., Braskie, M.N., Hua, X., Apostolova, L.G., Leow, A.D., Thompson, P.M., Ringman, J.M., 2013. Regional brain volume differences in symptomatic and presymptomatic carriers of familial Alzheimer's disease mutations. J. Neurol. Neurosurg. Psychiatry 84, 154–162.

Lerch, J.P., Carroll, J.B., Dorr, A., Spring, S., Evans, A.C., Hayden, M.R., Sled, J.G., Henkelman, R.M., 2008. Cortical thickness measured from MRI in the YAC128 mouse model of Huntington's disease. Neuroimage 41, 243–251.

Lerch, J.P., Yiu, A.P., Martinez-Canabal, A., Pekar, T., Bohbot, V.D., Frankland, P.W., Henkelman, R.M., Josselyn, S.A., Sled, J.G., 2011a. Maze training in mice induces MRI-detectable brain shape changes specific to the type of learning. Neuroimage 54, 2086–2095.

Lerch, J.P., Sled, J.G., Henkelman, R.M., 2011b. MRI phenotyping of genetically altered mice. Methods Mol. Biol. 711, 349–361.

Lerch, J.P., Gazdzinski, L., Germann, J., Sled, J.G., Henkelman, R.M., Nieman, B.J., 2012. Wanted dead or alive? The tradeoff between in-vivo versus ex-vivo MR brain imaging in the mouse. Front. Neuroinform. 6, 6.

Li, J., Wang, Y.J., Zhang, M., Xu, Z.Q., Gao, C.Y., Fang, C.Q., Yan, J.C., Zhou, H.D., 2011. Vascular risk factors promote conversion from mild cognitive impairment to Alzheimer disease. Neurology 76, 1485–1491.

Maguire, E.A., Gadian, D.G., Johnsrude, I.S., Good, C.D., Ashburner, J., Frackowiak, R.S., Frith, C.D., 2000. Navigation-related structural change in the hippocampi of taxi drivers. Proc. Natl. Acad. Sci. U. S. A. 97, 4398–4403.

Maheswaran, S., Barjat, H., Rueckert, D., Bate, S.T., Howlett, D.R., Tilling, L., Smart, S.C., Pohlmann, A., Richardson, J.C., Hartkens, T., Hill, D.L., Upton, N., Hajnal, J.V., James, M.F., 2009. Longitudinal regional brain volume changes quantified in normal aging and Alzheimer's APP × PS1 mice using MRI. Brain Res. 1270, 19–32.

Maviel, T., Durkin, T.P., Menzaghi, F., Bontempi, B., 2004. Sites of neocortical reorganization critical for remote spatial memory. Science 305, 96–99.

Morris, R., 1984. Developments of a water-maze procedure for studying spatial learning in the rat. J. Neurosci. Methods 11, 47–60.

Moser, M.B., Moser, E.I., Forrest, E., Andersen, P., Morris, R.G., 1995. Spatial learning with a minislab in the dorsal hippocampus. Proc. Natl. Acad. Sci. U. S. A. 92, 9697–9701.

Mucke, L., Masliah, E., Yu, G.Q., Mallory, M., Rockenstein, E.M., Tatsuno, G., Hu, K., Kholodenko, D., Johnson-Wood, K., McConlogue, L., 2000. High-level neuronal expression of abeta 1–42 in wild-type human amyloid protein precursor transgenic mice: synaptotoxicity without plaque formation. J. Neurosci. 20, 4050–4058.

Nicolakakis, N., Aboulkassim, T., Ongali, B., Lecrux, C., Fernandes, P., Rosa-Neto, P., Tong, X.K., Hamel, E., 2008. Complete rescue of cerebrovascular function in aged Alzheimer's disease transgenic mice by antioxidants and pioglitazone, a peroxisome proliferator-activated receptor gamma agonist. J. Neurosci. 28, 9287–9296.

Niwa, K., Younkin, L., Ebeling, C., Turner, S.K., Westaway, D., Younkin, S., Ashe, K.H., Carlson, G.A., Iadecola, C., 2000. Abeta 1–40-related reduction in functional hyperemia in mouse neocortex during somatosensory activation. Proc. Natl. Acad. Sci. U. S. A. 97, 9735–9740.

Niwa, K., Kazama, K., Younkin, S.G., Carlson, G.A., Iadecola, C., 2002. Alterations in cerebral blood flow and glucose utilization in mice overexpressing the amyloid precursor protein. Neurobiol. Dis. 9, 61–68.

O'Brien, R.J., Resnick, S.M., Zonderman, A.B., Ferrucci, L., Crain, B.J., Pletnikova, O., Rudow, G., Iacono, D., Riudavets, M.A., Driscoll, I., Price, D.L., Martin, L.J., Troncoso, J.C., 2009. Neuropathologic studies of the Baltimore Longitudinal Study of Aging (BLSA). J. Alzheimers Dis. 18, 665–675.

Oh, E.S., Savonenko, A.V., King, J.F., Fangmark Tucker, S.M., Rudow, G.L., Xu, G., Borchelt, D.R., Troncoso, J.C., 2009. Amyloid precursor protein increases cortical neuron size in transgenic mice. Neurobiol. Aging 30, 1238–1244.

Paxinos, G., Franklin, K.B.J., 2001. The Mouse Brain in Stereotaxic Coordinates. Academic, San Diego, Calif.; London.

Peters, F., Collette, F., Degueldre, C., Sterpenich, V., Majerus, S., Salmon, E., 2009. The neural correlates of verbal short-term memory in Alzheimer's disease: an fMRI study. Brain 132, 1833–1846.

Pinheiro, J.C., Bates, D.M., 2000. Mixed-effects Models in S and S-PLUS. Springer, New York; London.

Redwine, J.M., Kosofsky, B., Jacobs, R.E., Games, D., Reilly, J.F., Morrison, J.H., Young, W.G., Bloom, F.E., 2003. Dentate gyrus volume is reduced before onset of plaque formation in PDAPP mice: a magnetic resonance microscopy and stereologic analysis. Proc. Natl. Acad. Sci. U. S. A. 100, 1381–1386.

Richards, K., Watson, C., Buckley, R.F., Kurniawan, N.D., Yang, Z., Keller, M.D., Beare, R., Bartlett, P.F., Egan, G.F., Galloway, G.J., Paxinos, G., Petrou, S., Reutens, D.C., 2011. Segmentation of the mouse hippocampal formation in magnetic resonance images. Neuroimage 58, 732–740.

Riudavets, M.A., Iacono, D., Resnick, S.M., O'Brien, R., Zonderman, A.B., Martin, L.J., Rudow, G., Pletnikova, O., Troncoso, J.C., 2007. Resistance to Alzheimer's pathology is associated with nuclear hypertrophy in neurons. Neurobiol. Aging 28, 1484–1492.

Rochefort, C., Lefort, J., Rondi-Reig, L., 2013. The cerebellum: a new key structure in the navigation system. Front. Neural Circuits 7, 35.

Rodriguez, G., Vitali, P., Calvini, P., Bordoni, C., Girtler, N., Taddei, G., Mariani, G., Nobili, F., 2000. Hippocampal perfusion in mild Alzheimer's disease. Psychiatry Res. 100, 65–74.

Ros, J., Pellerin, L., Magara, F., Dauguet, J., Schenk, F., Magistretti, P.J., 2006. Metabolic activation pattern of distinct hippocampal subregions during spatial learning and memory retrieval. J. Cereb. Blood Flow Metab. 26, 468–477.

Sato, T., Hanyu, H., Hirao, K., Kanetaka, H., Sakurai, H., Iwamoto, T., 2009. Efficacy of PPAR-gamma agonist pioglitazone in mild Alzheimer disease. Neurobiol. Aging 32, 1626–1633.

Scahill, R.I., Ridgway, G.R., Bartlett, J.W., Barnes, J., Ryan, N.S., Mead, S., Beck, J., Clarkson, M.J., Crutch, S.J., Schott, J.M., Ourselin, S., Warren, J.D., Hardy, J., Rossor, M.N., Fox, N.C., 2013. Genetic influences on atrophy patterns in familial Alzheimer's disease: a comparison of APP and PSEN1 mutations. J. Alzheimers Dis. 35, 199–212.

Suthana, N.A., Ekstrom, A.D., Moshirvaziri, S., Knowlton, B., Bookheimer, S.Y., 2009. Human hippocampal CA1 involvement during allocentric encoding of spatial information. J. Neurosci. 29, 10512–10519.

Thompson, R.F., 2000. The Brain: A Neuroscience Primer. Worth, New York.

Vann, S.D., Aggleton, J.P., 2003. Evidence of a spatial encoding deficit in rats with lesions of the mammillary bodies or mammillothalamic tract. J. Neurosci. 23, 3506–3514.

Vann, S.D., Albasser, M.M., 2011. Hippocampus and neocortex: recognition and spatial memory. Curr. Opin. Neurobiol. 21, 440–445.

Villain, N., Desgranges, B., Viader, F., de la Sayette, V., Mezenge, F., Landeau, B., Baron, J.C., Eustache, F., Chetelat, G., 2008. Relationships between hippocampal atrophy, white matter disruption, and gray matter hypometabolism in Alzheimer's disease. J. Neurosci. 28, 6174–6181.

Warburton, E.C., Aggleton, J.P., Muir, J.L., 1998. Comparing the effects of selective cingulate cortex lesions and cingulum bundle lesions on water maze performance by rats. Eur. J. Neurosci. 10, 622–634.

Wegiel, J., Wisniewski, H.M., Dziewiatkowski, J., Badmajew, E., Tarnawski, M., Reisberg, B., Mlodzik, B., De Leon, M.J., Miller, D.C., 1999. Cerebellar atrophy in Alzheimer's disease-clinicopathological correlations. Brain Res. 818, 41–50.

Woollett, K., Maguire, E.A., 2011. Acquiring "the Knowledge" of London's layout drives structural brain changes. Curr. Biol. 21, 2109–2114.

Wright, A.L., Zinn, R., Hohensinn, B., Konen, L.M., Beynon, S.B., Tan, R.P., Clark, I.A., Abdipranoto, A., Vissel, B., 2013. Neuroinflammation and neuronal loss precede abeta plaque deposition in the hAPP-J20 mouse model of Alzheimer's disease. PLoS One 8, e59586.

Xu, G., Antuono, P.G., Jones, J., Xu, Y., Wu, G., Ward, D., Li, S.J., 2007. Perfusion fMRI detects deficits in regional CBF during memory-encoding tasks in MCI subjects. Neurology 69, 1650–1656.

Yoshida, T., Ha-Kawa, S., Yoshimura, M., Nobuhara, K., Kinoshita, T., Sawada, S., 2007. Effectiveness of treatment with donepezil hydrochloride and changes in regional cerebral blood flow in patients with Alzheimer's disease. Ann. Nucl. Med. 21, 257–265.

Zlokovic, B.V., Deane, R., Sallstrom, J., Chow, N., Miano, J.M., 2005. Neurovascular pathways and Alzheimer amyloid beta-peptide. Brain Pathol. 15, 78–83.